Biochimica et Biophysica Acta 1827 (2013) 761–768

Contents lists available at SciVerse ScienceDirect

Biochimica et Biophysica Acta

journal homepage: www.elsevier.com/locate/bbabio

Key role of water in proton transfer at the Q_o-site of the cytochrome bc_1 complex predicted by atomistic molecular dynamics simulations

Pekka A. Postila [a], Karol Kaszuba [a], Marcin Sarewicz [b], Artur Osyczka [b], Ilpo Vattulainen [a,c], Tomasz Róg [a,*]

[a] Department of Physics, Tampere University of Technology, P.O. Box 692, FI-33101 Tampere, Finland
[b] Department of Molecular Biophysics, Faculty of Biochemistry, Biophysics and Biotechnology, Jagiellonian University in Krakow, Gronostajowa 7, 30-387 Kraków, Poland
[c] MEMPHYS Center for Biomembrane Physics, University of Southern Denmark, Odense, Denmark

ARTICLE INFO

Article history:
Received 28 November 2012
Received in revised form 24 January 2013
Accepted 11 February 2013
Available online 18 February 2013

Keywords:
Cytochrome bc_1
Molecular dynamics simulation
Quinol/quinone
Electron transfer
Proton transfer
Short-circuit suppression

ABSTRACT

Cytochrome (cyt) bc_1 complex, which is an integral part of the respiratory chain and related energy-conserving systems, has two quinone-binding cavities (Q_o- and Q_i-sites), where the substrate participates in electron and proton transfer. Due to its complexity, many of the mechanistic details of the cyt bc_1 function have remained unclear especially regarding the substrate binding at the Q_o-site. In this work we address this issue by performing extensive atomistic molecular dynamics simulations with the cyt bc_1 complex of *Rhodobacter capsulatus* embedded in a lipid bilayer. Based on the simulations we are able to show the atom-level binding modes of two substrate forms: quinol (QH_2) and quinone (Q). The QH_2 binding at the Q_o-site involves a coordinated water arrangement that produces an exceptionally close and stable interaction between the cyt *b* and iron sulfur protein subunits. In this arrangement water molecules are positioned suitably in relation to the hydroxyls of the QH_2 ring to act as the primary acceptors of protons detaching from the oxidized substrate. In contrast, water does not have a similar role in the Q binding at the Q_o-site. Moreover, the coordinated water molecule is also a prime candidate to act as a structural element, gating for short-circuit suppression at the Q_o-site.

1. Introduction

Cytochrome (cyt) bc_1 (mitochondrial complex III; Fig. 1A) is a multi-subunit energy-conserving complex, which operates in the inner mitochondrial membrane of eukaryotes and in the plasma membrane of bacteria. It is an integral part of respiratory or photosynthetic chains, where it reversibly transfers electrons from substrate quinol (QH_2) to cyt *c*, which is coupled to translocation of protons across the bioenergetic membrane [1,2]. The reaction mechanism of the cyt bc_1 complex, also referred to as the Q-cycle, results in net oxidation of two QH_2 molecules with release of four protons to the positive side of the membrane, and reduction of one quinone (Q) with uptake of two protons from the negative side (Fig. 1). The importance of understanding the mechanisms underlying the electron and proton transfers associated with the complex is highlighted by the fact that the Q-cycle is largely the heart of cell function. It contributes to generation of the proton motive force, which is used to maintain the life-sustaining intracellular ATP/ADP ratio [3].

The cyt bc_1 complexes contain three commonly shared catalytic subunits: cyt *b*, cyt c_1, and iron sulfur protein (ISP or Rieske protein) positioned symmetrically on both sides of a dimer (Fig. 1A). The reaction mechanism begins at the Q_o-site (Fig. 1B–C), which is situated between low potential heme (b_L; part of cyt *b*) and 2-iron 2-sulfur cluster (Fe_2S_2; part of ISP) prosthetic redox centers (Fig. 1B and D). The electrons derived from the fully protonated substrate QH_2 at the Q_o-site are routed to two pathways: 1) one electron moves *via* the Fe_2S_2 cluster and the heme c_1 (part of cyt c_1) to the cyt c_1 subunit, and 2) the other electron is transferred *via* the heme b_L and high potential heme (b_H; part of cyt *b*) to the non-protonated Q in the Q_i-site located on the opposite side of the membrane [2,4]. In addition to electron transfer occurring within the monomer, electrons can be exchanged between the monomers through a bridge formed by the two heme b_L groups [5–8]. Thus, two Q_o-sites on both sides of the dimer are linked in an H-shaped electron transfer system (Fig. 1D) with four QH_2/Q oxidation/reduction terminals [7]. The exact mode of operation of this system is intensely being debated and, consequently, several (often mutually exclusive) scenarios of the operation of the dimer have been suggested [9–12].

Because of the bifurcated nature of the electron transfer process, two QH_2 molecules need to be oxidized at the Q_o-site to fully reduce a single Q molecule into QH_2 at the Q_i-site (Figs. 2D and 2). The half-reduced reaction intermediate known as semiquinone (SQ) has been detected at the Q_i-site [13,14]. While trapping this substrate form at the Q_o-site has proven very difficult, SQ associated with the Q_o-site has recently been observed in experiments [15,16]. As for its structure, SQ has both a hydroxyl and oxygen-centered radical attached to its ring system (Fig. 2). The substrate's C2-positioned

* Corresponding author. Tel.: +358 40 198 1179.
E-mail address: tomasz.rog@tut.fi (T. Róg).

0005-2728/$ – see front matter © 2013 Elsevier B.V. All rights reserved.
http://dx.doi.org/10.1016/j.bbabio.2013.02.005

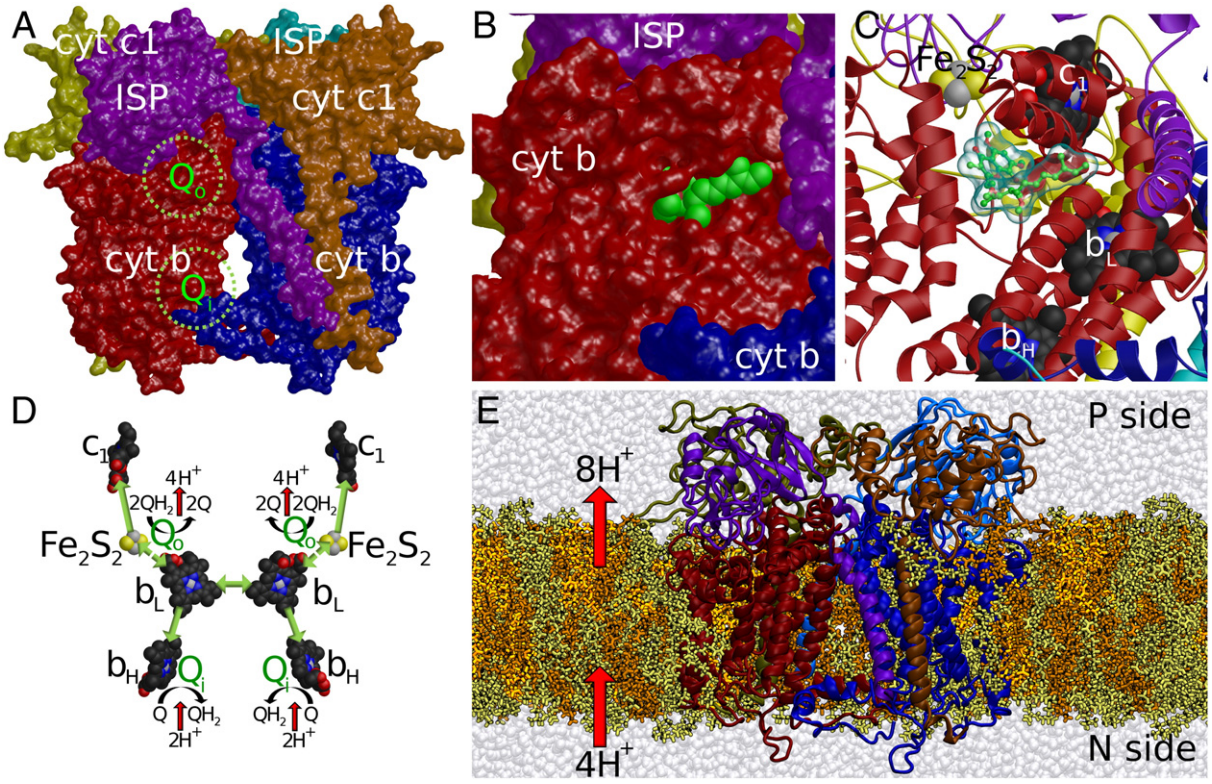

Fig. 1. The cytochrome bc_1 complex. A) The protein dimer [21] consisting of cyt *b* (red and blue), cyt c_1 (yellow and orange), and iron sulfur protein (ISP; cyan and magenta) subunits are shown using an opaque surface. The general positions of Q_o-and Q_i-sites are shown on one side of the dimer with green dotted circle. B) A close-up of the cyt *b* surface shows the bound inhibitor stigmatellin (green CPK) sticking out from the Q_o-site. C) A cartoon representation of the Q_o-site (same angle as in panel B) shows the position of the inhibitor (green ball-and stick with blue transparent surface) in relation to heme c_1, 2-iron 2-sulfur (Fe_2S_2) cluster, low potential heme (b_L), and high potential heme (b_H) prosthetic redox centers (CPKs). D) The Q_o-sites are positioned between the Fe_2S_2 cluster and the heme b_L on both sides of the dimer, whereas the Q_i-sites are next to the heme b_H groups in the dimer interface. The green arrows indicate directions of electron transfers within the system. At the Q_o-site quinols (QH_2s) are oxidized to quinones (Qs) but at the Q_i-site Qs are reduced to QH_2s. E) The simulated cyt bc_1 complex (cartoon) is shown embedded into a lipid bilayer (licorices) and solvated with explicit solvent (transparent CPKs). Two simultaneous Q-cycles on both sides of the dimer (see panel D) pushes altogether eight protons (H^+) into the positive (P) side and removes four into the negative (N) side.

isoprene tail (Fig. 2), whose length varies (~6–10 units) depending on the origin of the complex [17], ensures that the Q/QH_2 reservoir is confined into the membrane to efficiently shuttle electrons between various components of electron transfer chains and/or act as an antioxidant [18].

Numerous X-ray crystal structures for bovine, chicken, yeast, and bacterial cyt bc_1 complexes have been solved (Table S1). The data strongly suggest that the association of the flexible ISP-domain with the cyt *b* subunit across the Q_o-site is required for the Q-cycle [19]. However, the intricate mechanisms of the complex operation at the site are still unknown. Accordingly, the Q_o-sites have only been crystallized with inhibitors such as stigmatellin (Fig. 1B and C; Fig. 2) or without any compound (*apo*). Therefore, the exact binding modes of the QH_2/SQ/Q or electron/proton transfer steps associated with oxidation of QH_2 at the Q_o-site remain unidentified. The general view has been that the substrate would position itself at the Q_o-site roughly the same way as stigmatellin (Fig. 1B–C), which bind into the cavity with a considerably higher affinity than the substrate [20].

In this work, we consider this issue from computational viewpoint to acquire a fresh perspective on Q-mediated electron/proton transfer process — an issue that the static crystal structures of the inhibitor-bound complexes cannot address.

Our primary objective is to enlighten the elusive issue of substrate binding at the Q_o-site by simulating the entire cyt bc_1 complex of the purple photosynthetic bacterium *Rhodobacter capsulatus* (Fig. 1A and E; [21]) using classical all-atom molecular dynamics (MD) simulations. This bacterial complex contains the same catalytic core consisting of six subunits (Fig. 1A) as its mitochondrial counterparts, missing only the additional subunits that do not contain cofactors and are not directly involved in the catalytic reactions [21]. Even with this minimal core the computational effort and the complexity of the MD simulation set-up is formidable [22]. Both solvation and embedding of the protein into the lipid bilayer are essential, since otherwise there is no means to realistically mimic the *in situ* surroundings of the complex inside a membrane (Fig. 1E). Based on the simulations we present herein binding modes for both Q and QH_2 (Fig. 2) inside the Q_o-site at the atomistic level. Principally, our results show that water molecules are vital for the QH_2 binding by assuring close cyt *b*-ISP interaction and likely facilitating the proton transfer at the Q_o-site.

2. Methods

2.1. Preparation of three biologically relevant simulation configurations

The cyt bc_1 complex was prepared for three molecular dynamics (MD) simulations. These configurations differed in their redox states of the prosthetic groups and the occupancy of the Q_o- and Q_i-sites (Table 1). In the $conf_1$ set-up the Q_o-site was unoccupied (*apo*), but the Q_i-site contained the inhibitor antimycin. The redox state of the cofactors was set according to their midpoint potentials, assuming exposure to ambient redox potentials in air. Accordingly, the high potential redox centers (heme c_1, Fe_2S_2 cluster) were set to be reduced, while the low potential cofactors (heme b_L, heme b_H) were set at the oxidized states. The $conf_2$ set-up represents a state of the complex primed for the first turnover of the Q-cycle: the Q_o- and Q_i-sites both had bound substrates, QH_2 and Q, respectively, and all redox centers were set at the oxidized states. Finally, the $conf_3$ set-up represents a state of the complex immediately after oxidation of QH_2 at the

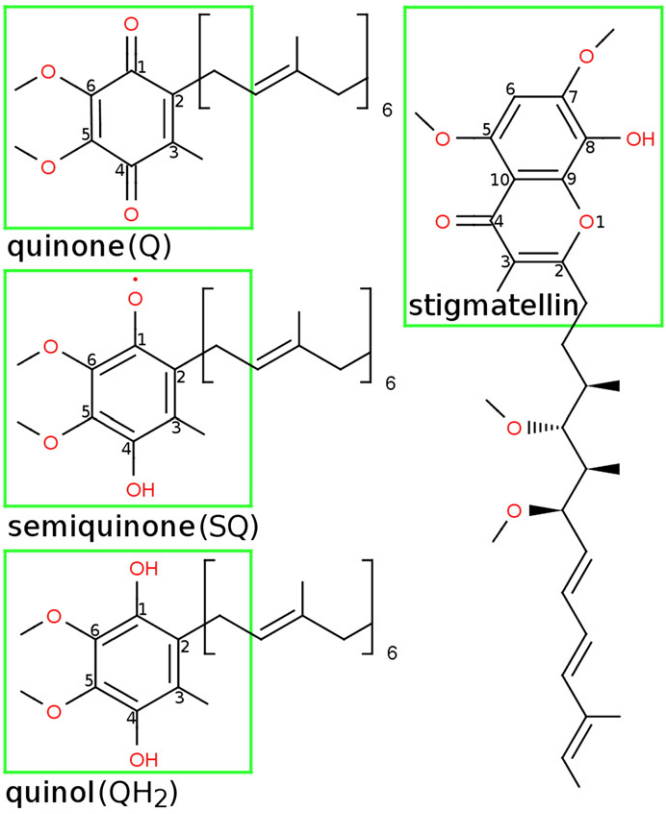

Fig. 2. The 2D ligand structures. The non-protonated substrate quinone (Q), the half-protonated radical semiquinone (SQ), the fully protonated substrate quinol (QH_2), and the Q_o-site-specific inhibitor stigmatellin. The head group considered in the RMSD calculations is boxed (Table S5).

Q_o-site during the second turnover of the Q-cycle. Here, the product, Q, has not yet left the Q_o-site, the heme b_L and the Fe_2S_2 cluster are both reduced, and the Q_i-site is occupied by a bound SQ (product of the first turnover; Fig. 2). Regarding the Q_o-site, the His156 side chain (part of ISP subunit) was set epsilon protonated and Glu295 side chain (part of cyt *b*) deprotonated in all configurations similarly as in the inhibitor-bound X-ray crystal structure [21].

2.2. System build-up for simulations

The systems were built with VMD1.9 [23] by using the stigmatellin-bound X-ray crystal structure (PDB ID: 1ZRT; [21]) as the starting conformation. The inhibitor-bound structure was an ideal choice for running the substrate-bound simulations, because stigmatellin's structural properties remind closely those of the substrate (see Fig. 2). The inhibitor molecules were either removed or replaced with the substrate forms at the Q_o-site on each side of the dimer (Table 1; Fig. 1B–C). Regarding the dimer, the letter A refers to a monomer composed of chains C (cyt *b*), D (cyt c_1), and R (ISP), and letter B to chains P (cyt *b*), Q (cyt c_1), and E (ISP) in the crystal structure (Fig. 1A). The ligand–protein complexes were embedded into lipid bilayers consisting of 102 cardiolipin (CL 18:2/18:2/18:2/18:2), 406 phosphatidylcholine (PC 18:2/18:2), and 342 phosphatidylethanolamine (PE 18:2/18:2) lipids. The system was solvated with TIP3P water molecules; those waters that overlapped with the membrane or the protein were removed. The negative charge of the system was neutralized with Na^+ ions. The system (~500,000 atoms in total) included the cyt bc_1 protein, 850 lipids, ~115,000 water molecules, 238–244 Na^+ ions depending on the configuration (242 $conf_1$, 238 $conf_2$, 244 $conf_3$), and the bound substrates/inhibitors. The dimensions were 162 Å × 142 Å × 132 Å, in X, Y, and Z directions, respectively.

2.3. Molecular dynamics simulations

The 200 ns MD simulations were performed using NAMD2.7 [24] employing the CHARMM 22 force-field parameters for the protein with the CMAP [25] correction map for main chain dihedrals, and CHARMM 27 parameters for lipids with later modification [26]. Lipid bilayer structure was taken from our previous studies [27,28]. The time step was 1 fs and short range non-bonded forces were considered every 2 fs. Long-range electrostatic interactions were calculated using the smooth particle mesh Ewald method [29]. Full periodic boundary conditions were used. The protein–protein distance in the neighboring images was at least two times larger than the 12 Å cut-off distance for van der Waals interactions. The target temperature was 310 K and target pressure 1 atm. The same simulation protocol was used in our previous study [30].

As the emphasis of this study is on the Q_o-site dynamics, we describe the development of the used CHARMM force-field parameters for the redox centers and ligands elsewhere [22]. Likewise, results for the Q_i-site or lipid-protein interactions will be discussed in following studies. Details of analyses and figure preparation are described in the supplementary material.

3. Results

3.1. The Q_o-site preserved without a bound inhibitor

The inhibitor-bound Q_o-site is a clearly defined invagination in the original X-ray crystal structure used in the simulations (Fig. 1B–C; Fig. 3A; [21]). Although the cavity shrinks and the residues rotate in the *apo* state, the main cavity formerly occupied by stigmatellin (Fig. 3A) is mostly preserved during the $conf_1$ simulation (Table 1; Fig. 3B). None of the dynamic changes suggest that there would be enough room in this cavity for more than one substrate (Fig. 3; discussed in Refs. [31–33]). Solvent did not move into the region where stigmatellin's tail lies (right panels in Fig. 3B) even though water flow in the vicinity of the main chain oxygen of the Cys155 (or Cys155°), Pro154° (part of ISP), Ile292°, and Tyr302 side chain (part of cyt *b*; left panels Fig. 3B). Glu295 side chain (part of the conserved PEWY motif in the cyt *b* subunit) rotated out of the cavity to hydrogen bond (H-bond) with water molecules (Fig. 3B). The solvent-accessible surface area (SASA) calculations indicated that the cyt *b*-iron sulfur protein (ISP) interface moved more in the *apo* simulation, at least on the A side (blue line in Fig. S1C; Table S2), than in the substrate-bound complexes (red and green lines in Fig. S1; Table S2). On the other hand, the Fe_2S_2 cluster-heme b_L distance generally did not change (~26 Å; Table S3) and the amount of direct H-bonding between the ISP and cyt *b* subunits remained quite high (Table S4).

Table 1
The molecular dynamics simulation set-ups of cytochrome bc_1 complex.

MD simulation configuration	Q_i-site inhibitor or substrate	Q_o-site substrate	Heme b_L[a]	Heme b_H[a]	Heme c_1[a]	Fe_2S_2 cluster[a]
$conf_1$	Antimycin	*apo*	−1 ox	−1 ox	−2 red	−1 red
$conf_2$	Quinone	Quinol	−1 ox	−1 ox	−1 ox	0 ox
$conf_3$	Semiquinone	Quinone	−2 red	−1 ox	−1 ox	−1 red

[a] The formal charge of the redox centers: red = reduced and ox = oxidized.

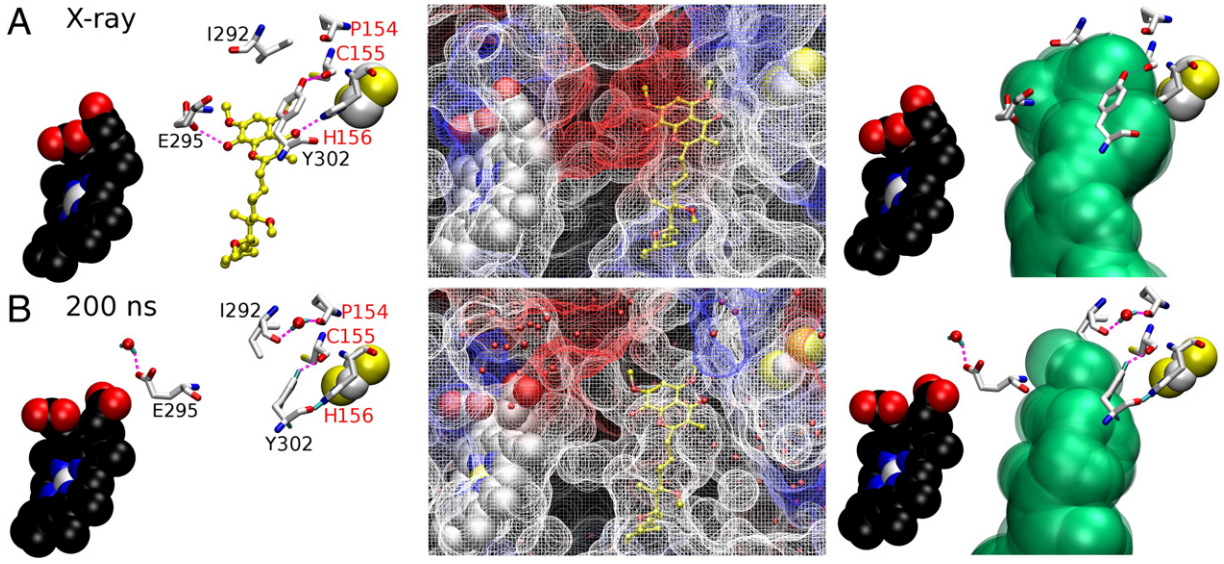

Fig. 3. Shape of the Q_o-site with an inhibitor and without a bound ligand. A) In the crystal structure [21], the inhibitor stigmatellin (yellow ball-and-stick; left) H-bonds with the side chains of His156 and Glu295. The protein surface potential calculated using Poisson–Boltzmann electrostatics indicates that the upper part of the Q_o-site (water-accessible mesh; middle) is more polar (red = negative; blue = positive) than the lower part, where stigmatellin's hydrophobic tail lies (white = neutral). The Q_o-site, whose shape matches the inhibitor's conformation, is presented in a simplified form as a main cavity (green CPK; right). B) At 200 ns of the *apo*-Q_o simulation ($conf_1$; Table 1), Ile294° and Pro154° are H-bonded *via* a water bridge (left) linking the cyt *b* and ISP subunits. The Glu295 side chain turned out of the cavity to interact with water molecules. The protein surface potential also changed to more neutral state. Although the Q_o-site as a whole (middle) and the main cavity (green CPK; right) changed shape without the inhibitor, stigmatellin would still almost fit inside (middle). The labels of residues from the cyt *b* are in black and the ones from the ISP are shown in red. Both the heme b_L and the Fe_2S_2 cluster are shown (CPKs; Fig. 1D).

3.2. Quinol binding at the Q_o-site involves a coordinated water molecule

The quinol (QH_2) binding (yellow in Fig. 4A–D) mode did not deviate much from the stigmatellin's alignment seen in the crystal structure (green in Figs. 1B and C) even in the later stages of the $conf_2$ simulation (pink in Fig. 4D). Root mean square deviation (RMSD) calculations indicated that the isoprene tail of QH_2, sandwiched between hydrophobic residues and lipid tails (Fig. 4C), was in general more mobile

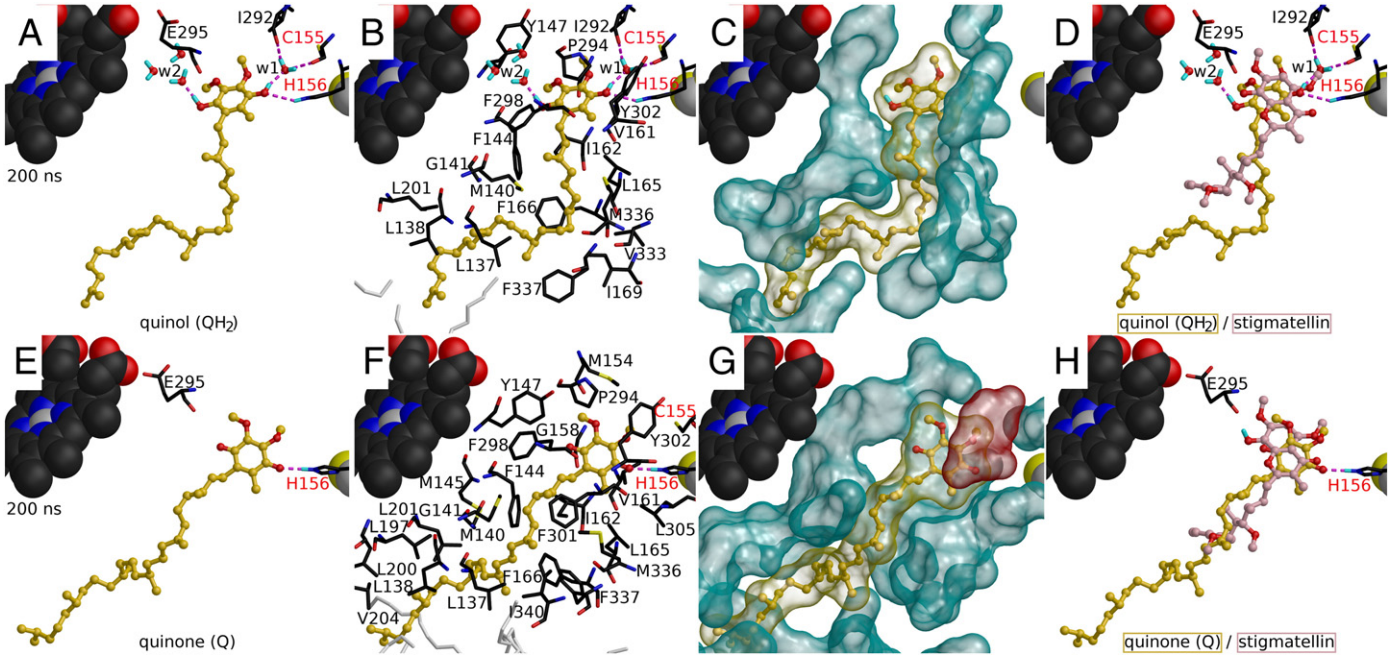

Fig. 4. Quinol and quinone binding at the Q_o-site at 200 ns. A) In the $conf_2$ simulation both the C1- and the C4-hydroxyls of quinol (QH_2; yellow ball-and-stick) H-bond (magenta dashed lines) with waters w2 and w1, respectively. The w1 donates its hydrogen atoms (cyan sticks) for the main chain oxygen of Ile292 and Cys155, while its lone pair receives a hydrogen from the C4-hydroxyl. Furthermore, the QH_2's C4-hydroxyl H-bonds with His156 (Fig. S2; Table S6). B) In addition to the main H-bonding partners the QH_2 also interacts with several steric residues (black sticks) and lipid molecules (white sticks) in induced fit manner. C) The hydrophobic residue alignment (transparent blue surface) complements QH_2's shape (transparent yellow surface). D) The final alignment of QH_2's tail reminds that of stigmatellin's tail (pink ball-and-stick) in the crystal structure. E) In the $conf_3$ simulation the H-bond with the carboxyl group of Glu295 is not possible with a bound quinone (Q; yellow ball-and-stick) as its C1-carbonyl is also an H-bond acceptor. The H-bond between the C4-carbonyl and His156 is formed directly without water involvement (Fig. S2C; Table S6). F) The final alignment of cavity residues against Q reminded closely that of QH_2 at 200 ns (A vs. B), though there were dynamic differences. G) The hydrophobic alignment of QH_2 with the Q_o-site residues was mostly favorable (blue transparent surface), although Tyr302 (red transparent surface) was somewhat unfavorably positioned in this particular snap shot. H) The alignment of stigmatellin's tail reminds closely the alignment of Q's tail. The B side of the dimer was selected for both $conf_2$ (panels A–D) and $-_3$ (panels E–H) snapshots. See Fig. 3 for interpretation.

than the quinone ring with its coordinated polar substituents (Table S5). Of the two H-bonds initially present with the bound QH_2, the one between the carboxylate group of Glu295 and the C1-hydroxyl (equivalent to stigmatellin's C4-hydroxyl in Figs. 2 and 3A) was broken immediately as its side chain rotated to interact with water outside the main cavity (Fig. 4). The H-bond was formed momentarily again in the A side of the dimer at ~170 ns (Fig. S2A), which suggests that it could be possible *in situ* as well. The other H-bond formed between the epsilon protonated side chain of His156 (part of ISP subunit) and the lone pair of the C4-hydroxyl of QH_2 (donor; Fig. S2B; Fig. 4A; Table S6) was more stable throughout the simulation. Formation of the latter H-bond was possible because QH_2 positioned its C4-hydroxyl close to His156 (N—H···O—H) in a comparable manner as the C4-carbonyl of stigmatellin (N—H···O C) in the crystal structure (Fig. 4D).

Notably, the donor parts of the QH_2's C1- and C4-hydroxyls could only form H-bonds with solvent that flow into the cavity through the cyt *b*-ISP subunit interface. In fact, stable H-bonding between the QH_2's C4-hydroxyl (acceptor/donor) and the side chain of His156 (donor) required entry of a highly coordinated water molecule (w1 in Fig. 4A). This water molecule H-bonded with three groups: QH_2's C4-hydroxyl, Ile292° (part of cyt *b*), and Cys155° (part of ISP). The water arrangement in the QH_2 binding reminded the one in the *apo*-Q_o simulation (Fig. 3B). However, the QH_2 was also able to H-bond firmly with the His156 side chain. Because of this conserved water molecule's ability to "lock" itself and its interacting partners in the 3D space, stable H-bonding between the QH_2's C4-hydroxyl and the epsilon protonated His156 (part of ISP; red line in Fig. S2B; Table S6) was possible. In addition, the Fe_2S_2 cluster-heme b_L distance remained generally smaller than in the initial crystal structure (red line vs. black line in Fig. S1B), other simulated configurations, or in the available structures (Table S1). This shows that the ISP subunit was especially favorably positioned in relation to the cyt *b* – prerequisite for successful electron transfer at the Q_o-site (Table S2 vs. Table S3; [19]) – when the coordinated water was involved in the QH_2 binding (Fig. 4A).

Although the water stayed "locked" in the position ~85% of the simulation on the B side (Fig. S2D), equally tenable water engagement did not take place on the A side (Table S6), where the cyt *b*-ISP interaction was weaker (Tables S2–S4). Due to the weak interactions the substrate drifted momentarily away from its initial H-bonding partner His156 (blue line in Fig. S2B; Table S5). In the later stages of the simulation, C4-connected water molecule on the A side was able to shortly organize the same H-bonds as the coordinated water on the B side (Table S6). Because the Cys155° was not generally close enough to H-bond with a C4-connected water molecule, the site could be occupied by several erratically moving water molecules or even by the hydrophobic side chain of Ile292. This led to weaker H-bonding between QH_2's C4-hydroxyl and His156 on the A side, and between the cyt *b* and ISP subunits as well (Table S4). In the absence of the coordinated water, the Fe_2S_2 cluster-heme b_L distance also increased to a level where it was larger than in any other simulation (red line in Fig. S1A). Correspondingly, the contact area between the cyt *b* and ISP subunits then diminished considerably (red line in Fig. S1C). This alternative binding mode underlines the transient and implicit nature of the QH_2 binding at the Q_o-site, which could be the reason why the substrate-bound cavity has not been crystallized yet.

The C1-hydroxyl of QH_2 was also able to H-bond with transient water molecules, but none of them interacted in an equally coordinated manner as the C4-connected water (w1 in Fig. 4A). A water molecule (w2 in Fig. 4A) was at the H-bonding range with the C1-hydroxyl ~30% of the simulation on both sides of the dimer (Table S6). In general, a very loosely formed meshwork of water molecules connected the C1-hydroxyl to the heme b_L and to the side chain of Tyr297. Despite the differences in continuity of the H-bonds, both the C1- and C4-hydroxyls of QH_2 could be H-bonded to water molecules simultaneously (Fig. 4A; Table S6). We further note that of the two waters, only the C1-connected water (w2 in Fig. 4A; Table S6) is readily visible in some of the inhibitor-bound X-ray structures [34–40], where it is H-bonded both to the carboxylate group of Glu295 and to the hydroxyl group of an inhibitor. Thus, while there is indirect structural evidence for the placement of the C1-connected water (w2), there are no prior experimental data involving the C4-connected water (w1).

3.3. Quinone binding at the Q_o-site does not involve a water component

The alignment of quinone (Q) at the Q_o-site ($conf_3$; Table 1; Fig. 4E–H) reminded the positioning of stigmatellin in the crystal structure (Fig. 4H) and that of quinol (QH_2) in the $conf_2$ simulation (Fig. 4A–D vs. Fig. 4E–H). However, similarly favorable water-mediated interactions could not take place with Q as was seen for QH_2, because its ring system lacked the H-bond donor parts (Fig. 2) able to form H-bonds with the lone pairs of the water molecules' oxygen atoms (Fig. 4A). Neither of the simulated Q molecules strayed as far from the Fe_2S_2 cluster as the loosely bound QH_2 on the A side of the dimer in the $conf_2$ simulation (Fig. S2B vs. C). There was also a clear difference in the continuity of direct H-bonding between His156 and the C4-groups, if QH_2 and Q binding were compared (Fig. S2B vs. S2C; Table S6). This crucial H-bond was maintained more firmly in the Q–Q_o simulation on both sides of the dimer if compared to the QH_2–Q_o simulation. The H-bonding range was reached in ~46–87% of the 200 ns simulation depending on the inspected dimer side (Table S6). The firmer H-bond of Q was formed between His156 and the C4-carbonyl instead of the QH_2's C4-hydroxyl that is a relatively weak H-bond acceptor.

Although the RMSD values of QH_2 and Q did not differ markedly between simulations (Table S5), the QH_2 binding involving the coordinated water on the B side (w1 in Fig. 4A) produced more stable and closer cyt *b*-ISP subunit association than Q (Tables S2–S4). The C1-carbonyl of Q was unable to H-bond as there were no donors nearby (Fig. 4E), which likely caused some extra instability to the Q binding (Table S5). The foremost reason behind the less disturbed H-bonding between the C4-carbonyl and the side chain of His156 was the lack of solvent involvement in the Q binding. Notably, Ile292 (part of cyt *b*) kept moving throughout the Q–Q_o simulation as its main chain oxygen was not locked with respect to the ISP subunit by a coordinated water molecule. The lack of water-mediated interactions in Q–Q_o simulation also caused lower numbers of H-bonds to be formed at the cyt *b*-ISP interface in total if compared to the other simulations (Table S4). Because neither the C1- nor C4-carbonyl of Q H-bonded with water molecules, there were no solvent-mediated interactions to stabilize its binding, coordinate the cyt *b*-ISP subunit interactions, or temporally disrupt its H-bonding with His156. It is also important to recognize that the water coordination at the Q_o-site (w1 in Fig. 4A) would be equally impossible for QH_2 as it is for Q (Fig. 4D), if the His156 were in a deprotonated state upon substrate binding (discussed in Section 4.1).

3.4. Asymmetry in the dimer dynamics

A number of allosteric cooperation models for the dimeric enzyme have been suggested based on prior experiments [9,10]. In this respect, we did see that both the substrate binding and the redox center distances differed between the two dimer sides in our simulations (Fig. S1–S2, Tables S2–S6). It is, however, likely that the 200 ns simulations were not statistically representative enough to determine whether these asymmetrical movements followed a specific mechanism or resulted from random simulation effects. The latter option seems possible as phospholipid and solvent molecules, which were added when setting up the system, needed to adjust their positions in relation to the protein especially during the early steps of the simulations. Whatever the cause may be, the divergent behavior between the monomers shows at least that there is no strong tendency for concurrent movements between the dimer sides.

4. Discussion

4.1. What are the primary acceptors of protons at the Q_o-site?

Although the basics of the Q-cycle are well established [1–3], the lack of structural data involving the quinol (QH_2) or quinone (Q) binding at the Q_o-site has made it difficult to determine the atom-level interactions that govern the electron/proton transfer. Moreover, based on the inhibitor-bound X-ray crystal structures (Table S1) it has been difficult to pinpoint where the protons that detach from QH_2 go during the Q-cycle. It has been suggested that the side chains of His156 (part of ISP) and Glu295 (part of cyt *b*) initially acquire them [41,42], but their involvement in the proton transfer is problematic. First, site-directed mutagenesis, which has been possible only with Glu295, revealed that replacing the glutamate with a residue that is unable to accept protons (*e.g.* Glu295Val) or has an opposite formal charge (Glu295Lys) does not block the cycle but only modestly slows it down [43,44]. Second, these models require that His156 and/or Glu295 side chains would be deprotonated prior to the oxidation of QH_2. Although the charged state of Glu295 upon QH_2 binding is acceptable, the imidazolate state of the metal coordinated His156 remains debatable despite attempts to address it experimentally [45]. The conventional wisdom dictates that the totally deprotonated histidine can only exist in extreme conditions. In fact, the Q-cycle functions even in pH below 6 [12,46], which is the formal p*K*a value of histidine's imidazole side chain, suggesting constant epsilon protonation of the His156 during the entire catalytic cycle. Furthermore, the His156 side chain is also clearly epsilon protonated in the original crystal structure (Fig. 3A) with the bound inhibitor stigmatellin (Fig. 2) and, thus, it is difficult to argue why the protonation would differ so radically upon QH_2 binding. For these reasons we chose to use the epsilon protonated state of His156 and the deprotonated state of Glu295 in all of our atomistic simulations.

Meanwhile, the protons could be acquired by water molecules that form hydronium cations ($2H_2O + 2H^+ \rightarrow 2H_3O^+$; Fig. 5) during the electron transfer *via* the Fe_2S_2 cluster and the heme b_L (Fig. 1D). Prior to this study the involvement of water for the intraprotein proton transfer at the Q_o-site and for the close cyt *b*-ISP subunit association have just been speculated [41,47]. Nonetheless, this idea is well-founded as there is growing awareness that buried water molecules can play a key role in maintaining structural integrity of biological systems, mediating protein–protein interactions, and ultimately affecting the function as well [48]. For comparison, water molecules are known to lower the binding energies of drug molecules within intraprotein cavities [30,49], affect profoundly the cavity-ligand recognition [50], and coordinate ligand binding of numerous target proteins including ionotropic glutamate receptors [51–53], phosphodiesterases [54] and integrins [55] to mention a few. There exists a well-established case of non-random intraprotein proton transport from a substrate to coordinated water molecules at the bacteriorhodopsin's catalytic site [56]. It is also worth noting that at the Q_i-site, for which there exist X-ray structures with bound substrate, bridging waters have also been found [34] although they have not been suggested to take part in the proton transfer [57].

4.2. Water molecules meet the geometry criteria for intraprotein proton transfer

The explicit solvent is able to sample through proteins' water exchange pathways and cavities already within the first picoseconds of MD simulations [58]. Accordingly, we embedded the cyt bc_1 complex into a lipid bilayer (Fig. 1E) and allowed its inner parts to solvate freely during the energy minimization and relaxation steps of the simulations. This set-up, together with correct redox states of the cofactors and occupancy of the Q_o- and Q_i-sites (Table 1), assured that the protein was simulated as close to *in situ* conditions as possible. What is more, this arrangement was also needed for finding out without structural bias whether water molecules could be directly involved in the binding of the substrate forms and in the proton transfer steps. On the one hand, the freely spread water molecules did not approach the C1- and C4-carbonyl groups of bound Q at the Q_o-site in the $conf_3$ simulation (Fig. 4E). On the other hand, the C1- and C4-hydroxyls of bound QH_2 attracted water into the cavity (w1 and w2 in Fig. 4A) in the $conf_2$ simulation. One water molecule in particular acquired a highly coordinated position (w1 in Figs. 4A and S2D; Table S6) in which it H-bonded not only with QH_2's C4-hydroxyl but also with Ile292° (part of cyt *b*) and Cys155° (part of ISP). The C1-hydroxyl of QH_2 ($conf_2$; Table 1) can form H-bonds with transient waters that H-bond with yet more water molecules (Fig. 4A). This water-mediated interaction was not as constant as the C4-connected H-bonding (w1 vs. w2 in Table S6), but both the C1- and C4-hydroxyls of QH_2 could be bound to water at the same time. Hence, water molecules are positioned in suitable places, next to the C1- and C4-hydroxyls, where they could act as proton receiving partners in the two-electron oxidation process of QH_2 (Fig. 5).

4.3. A possible mechanism for short-circuit suppression

To efficiently convert energy, the cyt bc_1 complex must have a way to make sure that the catalytic reaction at the Q_o-site directs one electron from QH_2 to the high-potential chain ($QH_2 \rightarrow Fe_2S_2$ cluster → heme c_1 → cyt *c*; Fig. 1D), while the other is routed to the low-potential chain ($QH_2 \rightarrow$ heme $b_L \rightarrow$ heme $b_H \rightarrow$ Q/SQ, Fig. 1D). At the same time, there must be a safeguard mechanism that prevents the thermodynamically favorable backwards movement of the electrons between the chains

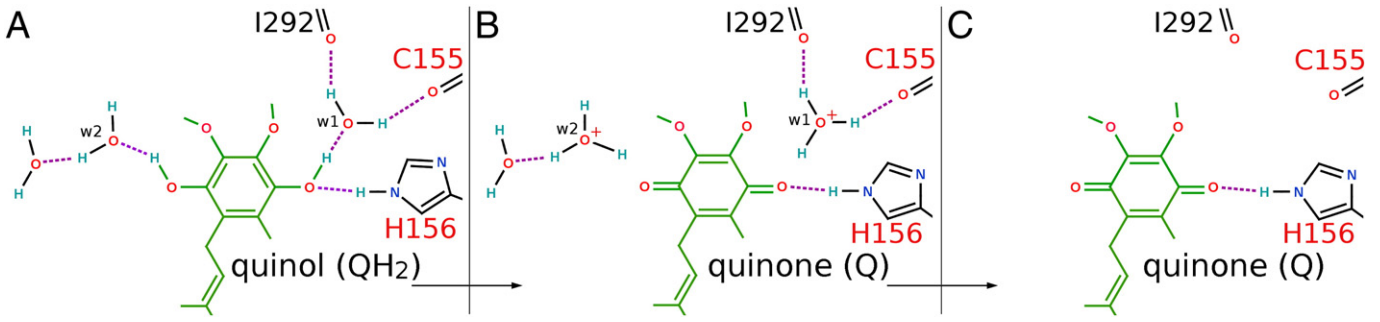

Fig. 5. How proton transfer from quinol to two water molecules could happen at the Q_o-site? A) A quinol (QH_2) molecule (green backbone) enters the Q_o-site and forms H-bonds (magenta dotted lines) with the side chain of His156 (part of ISP; black backbone) and two water molecules (w1 and w2 in Fig. 4A). The w1 molecule mediates interactions between the C4-hydroxyl, Ile292°, and Cys155° *via* H-bonds. The w2 molecule, seen also in several inhibitor-bound X-ray crystal structures (Table S1), forms H-bonds with the C1-hydroxyl. B) Next, two electrons are transferred from the oxidized QH_2 to the Fe_2S_2 cluster and the heme b_L, whereas two protons are acquired by the QH_2's C1- and C4-connected water molecules that turn into hydronium cations. C) Finally, the newly-generated cations leave the vicinity of the quinone (Q) ring's polar constituents (Fig. 4E). The presented scheme suggests routes for protons but not for the sequence of electron and proton transfer events (see Section 4.4 for further discussion). See Fig. 3 for interpretation.

across the Q_o-site. At present, the mechanism behind the short-circuit suppression remains unknown, but is intensely discussed especially in the context of its relation to the mechanism of generation of reactive oxygen species [12,59–61]. The simulation results are particularly relevant to one of the proposed scenarios in which a specific reorientation of water molecules as a function of redox state of the Fe_2S_2 cluster and the heme b_L would provide structural elements for gating the short-circuits [61].

Our results indicate how the short-circuit prevention may be accomplished at molecular level. The QH_2 simulation with the oxidized Fe_2S_2 cluster and heme b_L shows how the specific arrangement of a water molecule (w1 Fig. 4A) at the Q_o-site assures close contact between the cyt *b* and ISP subunits. This water-mediated arrangement does not take place if the substrate is oxidized and the redox centers in question are reduced as no water molecules approach the Q_o-site with bound Q (Fig. 4E). Thus, it seems reasonable to assume that the water-mediated H-bonding during QH_2 binding could be the mechanism behind the short-circuit prevention. Accordingly, it is likely that the optimal QH_2 binding mode involving the C1- and C4-connected water molecules is very short-lived and promotes close association of the cyt *b* and ISP subunits only before the oxidation of the substrate at the Q_o-site. Consequently, stable and close association of these subunits, needed for effective electron and proton transfer [19], could only be obtained *in situ* for a fleeting moment when the mediating partners, QH_2 and the C4-connected water molecule, are at the interface.

4.4. Suggested intraprotein proton transfer at the Q_o-site step by step

The water-mediated proton transfer could happen in a sequential or concerted manner at the Q_o-site [12,41,62]. The sequential mechanism dictates that one electron is transferred in two consecutive proton/electron transfer reactions ($QH_2 \rightarrow SQ + H^+/e^- \rightarrow Q + H^+/e^-$), whereas the concerted reaction would release both protons/electrons simultaneously ($QH_2 \rightarrow Q + 2H^+/2e^-$). Based on the simulations, we cannot say for sure what is the order of the transfers; however, we get an idea where the protons are routed. First, a QH_2 molecule enters the cavity and forms H-bonds with two waters (w1 and w2 in Figs. 4A and 5A) and His156 (Figs. 4A and 5A), which in turn promotes and/or follows the close association of the cyt *b* and ISP subunits (Fig. S1B and D). Second, the transfer of electrons from QH_2 to the Fe_2S_2 cluster and the heme b_L would be accompanied by a transfer of protons to the C1- and C4-connected water molecules that turn into hydronium cations (Fig. 5B). Finally, third, the newly-generated cations would flow out from the cavity, which would weaken the cyt *b*-ISP subunit association (Fig. 5C). Although not consistently seen in the QH_2–Q_o simulation (Fig. 4A–D; Table S6), the carboxylate group of Glu295 likely assists w2 coordination and proton transfer while H-bonding with the C1-hydroxyl (not shown in Fig. 5). It is possible that the Glu295 side chain is only involed in semiquinone (SQ) binding at the Q_o-site [41]. In this case, the SQ binding would mimic closely the established binding mode of stigmatellin (Fig. 3A) and the reaction would follow the sequential mechanism.

Even though the simulation results and the newly formed theory (Fig. 5) regarding the water involvement in the QH_2 binding should be tested using for example Fourier transform infrared difference spectroscopy, our work provides a working hypothesis that encompasses several key issues of the cyt bc_1 complex operation that have remained open over the years. The MD results provide a good premise for combined quantum mechanics/molecular mechanics (QM/MM) calculations to inspect actual proton transfer or its possible reversibility. The beauty of the suggested mechanism lies in its apparent simplicity and atom-level details. However, we expect that it will be challenging to verify the effect of the coordinated water (w1 in Figs. 4A and 5A) for the proton transfer or the short-circuit suppression using standard methods such as site-directed mutagenesis. This is because it is the main chain oxygen atoms of Ile292 or Cys155 that are interacting with the water in our simulations rather than their side chain substituents.

The ramifications of our findings are potentially substantial due to the cyt bc_1 complex's central position in the respiratory chain that affects the energy metabolism of a plethora of organisms ranging from bacteria to humans. Better understanding of the complex operation should lead to new insights regarding genetic defects that result in mitochondrial dysfunction, free radical generation affecting for example aging, or how the already established inhibitors actually function. Furthermore, our findings should make it more feasible to rationally design new drugs for a variety of cyt bc_1 complexes as we have a better grasp of its basic operation.

5. Conclusions

The 200 ns simulations indicate that the binding modes of quinol (QH_2) and quinone (Q) are alike with the inhibitor stigmatellin at the Q_o-site (Fig. 4D and H), but only the QH_2 binding involve a water component with both structural and functional implications. One water molecule acquired a coordinated position (w1 in Fig. 4A) that fixed QH_2's C4-hydroxyl, Ile292° (part of cyt *b*), and Cys155° (part of ISP) in a stable position *via* H-bonding interactions (Fig. S2D; Table S6). This rendered stable H-bonding possible between QH_2 and His156 side chain (Fig. S2B; Table S6) and assured greater stability in the cyt *b*-ISP interface as well (red lines in Figs. S1B and D; Tables S2–S4). The close spatial proximity of the two donor groups made QH_2 alignment unstable and the binding steadied only if the C4-connected water (w1 in Fig. 4A) assisted the substrate in coordinating the cyt *b*-ISP subunit association. Although the C1-hydroxyl of QH_2 was also able to H-bond with transient water molecules, it did not coordinate an H-bonding network that would have been as stable as the C4-hydroxyl (w1 vs. w2 in Fig. 4A). Adversely, the Q–Q_o simulation (Fig. 4E) clearly indicated that once the proton transfer from QH_2 is completed, water would not play a major role in the binding of the substrate. To sum up, our atomistic simulations suggest that water molecules are vital for the QH_2 binding by assuring close cyt *b*-ISP interaction, likely facilitating proton transfer (see Fig. 5) and the short-circuit suppression at the Q_o-site.

Acknowledgements

Computational resources were provided by CSC — IT Centre for Science (Espoo, Finland). We acknowledge that the results of this research have been in part achieved using the PRACE-2IP project (FP7 RI-283493) resource Lindgren based in Sweden at PDC. For financial support, we wish to thank the Academy of Finland (T.R., I.V., and P.A.P.), the Finnish Doctoral Programme in Computational Sciences (K.K.), and the European Research Council through the Advanced Grant (CROWDED-PRO-LIPIDS). A.O. acknowledges The Wellcome Trust International Senior Research Fellowship.

Appendix A. Supplementary data

Supplementary data to this article can be found online at http://dx.doi.org/10.1016/j.bbabio.2013.02.005.

References

[1] P. Mitchell, Protonmotive redox mechanism of the cytochrome b-c″1 complex in the respiratory chain: protonmotive ubiquinone cycle, FEBS Lett. 56 (1975) 1–6.
[2] U. Brandt, B. Trumpower, The protonmotive Q cycle in mitochondria and bacteria, Crit. Rev. Biochem. Mol. Biol. 29 (1994) 165–197.
[3] D.G. Nicholls, S.J. Ferguson, Bioenergetics 3, Academic Press, San Diego, Calif, 2002.
[4] E.A. Berry, M. Guergova-Kuras, L.S. Huang, A.R. Crofts, Structure and function of cytochrome bc complexes, Annu. Rev. Biochem. 69 (2000) 1005–1075.
[5] M. Castellani, R. Covian, T. Kleinschroth, O. Anderka, B. Ludwig, B.L. Trumpower, Direct demonstration of half-of-the-sites reactivity in the dimeric cytochrome bc1 complex: enzyme with one inactive monomer is fully active but unable to

activate the second ubiquinol oxidation site in response to ligand binding at the ubiquinone reduction site, J. Biol. Chem. 285 (2010) 502–510.
[6] P. Lanciano, D.-W. Lee, H. Yang, E. Darrouzet, F. Daldal, Intermonomer electron transfer between the low-potential b hemes of cytochrome bc , Biochemistry 50 (2011) 1651–1663.
[7] M. Swierczek, E. Cieluch, M. Sarewicz, A. Borek, C.C. Moser, P.L. Dutton, A. Osyczka, An electronic bus bar lies in the core of cytochrome bc1, Science 329 (2010) 451–454.
[8] M. Czapla, A. Borek, M. Sarewicz, A. Osyczka, Enzymatic activities of isolated cytochrome bc -like complexes containing fused cytochrome b subunits with asymmetrically inactivated segments of electron transfer chains, Biochemistry 51 (2012) 829–835.
[9] J.W. Cooley, D.-W. Lee, F. Daldal, Across membrane communication between the Q(o) and Q(i) active sites of cytochrome bc(1), Biochemistry 48 (2009) 1888–1899.
[10] R. Covian, B.L. Trumpower, Regulatory interactions in the dimeric cytochrome bc(1) complex: the advantages of being a twin, Biochim. Biophys. Acta 1777 (2008) 1079–1091.
[11] A.R. Crofts, J.T. Holland, D. Victoria, D.R.J. Kolling, S.A. Dikanov, R. Gilbreth, S. Lhee, R. Kuras, M.G. Kuras, The Q-cycle reviewed: how well does a monomeric mechanism of the bc(1) complex account for the function of a dimeric complex? Biochim. Biophys. Acta 1777 (2008) 1001–1019.
[12] A. Osyczka, C.C. Moser, F. Daldal, P.L. Dutton, Reversible redox energy coupling in electron transfer chains, Nature 427 (2004) 607–612.
[13] D.E. Robertson, R.C. Prince, J.R. Bowyer, K. Matsuura, P.L. Dutton, T. Ohnishi, Thermodynamic properties of the semiquinone and its binding site in the ubiquinol-cytochrome c (c2) oxidoreductase of respiratory and photosynthetic systems, J. Biol. Chem. 259 (1984) 1758–1763.
[14] S. Jünemann, P. Heathcote, P.R. Rich, On the mechanism of quinol oxidation in the bc1 complex, J. Biol. Chem. 273 (1998) 21603–21607.
[15] J.L. Cape, M.K. Bowman, D.M. Kramer, A semiquinone intermediate generated at the Qo site of the cytochrome bc1 complex: importance for the Q-cycle and superoxide production, Proc. Natl. Acad. Sci. U. S. A. 104 (2007) 7887–7892.
[16] H. Zhang, A. Osyczka, P.L. Dutton, C.C. Moser, Exposing the complex III Qo semiquinone radical, Biochim. Biophys. Acta 1767 (2007) 883–887.
[17] B. Nowicka, J. Kruk, Occurrence, biosynthesis and function of isoprenoid quinones, Biochim. Biophys. Acta, Bioenerg. 1797 (2010) 1587–1605.
[18] L. Ernster, P. Forsmark-Andrée, Ubiquinol: an endogenous antioxidant in aerobic organisms, Clin. Investig. 71 (1993) S60–S65.
[19] Z. Zhang, L. Huang, V.M. Shulmeister, Y.I. Chi, K.K. Kim, L.W. Hung, A.R. Crofts, E.A. Berry, S.H. Kim, Electron transfer by domain movement in cytochrome bc1, Nature 392 (1998) 677–684.
[20] H. Ding, D.E. Robertson, F. Daldal, P.L. Dutton, Cytochrome bc1 complex [2Fe-2S] cluster and its interaction with ubiquinone and ubihydroquinone at the Qo site: a double-occupancy Qo site model, Biochemistry 31 (1992) 3144–3158.
[21] E.A. Berry, L.-S. Huang, L.K. Saechao, N.G. Pon, M. Valkova-Valchanova, F. Daldal, X-ray structure of *Rhodobacter capsulatus* cytochrome bc (1): comparison with its mitochondrial and chloroplast counterparts, Photosynth. Res. 81 (2004) 251–275.
[22] K. Kaszuba, P.A. Postila, O. Cramariuc, M. Sarewicz, A. Osyczka, I. Vattulainen, T. Róg, Parameterization of the prosthetic redox centers of the bacterial cytochrome bc1 complex for atomistic molecular dynamics simulations, Theor. Chem. Accounts (in press).
[23] W. Humphrey, A. Dalke, K. Schulten, VMD: visual molecular dynamics, J. Mol. Graph. 14 (1996) 33–38, (27–8).
[24] J.C. Phillips, R. Braun, W. Wang, J. Gumbart, E. Tajkhorshid, E. Villa, C. Chipot, R.D. Skeel, L. Kalé, K. Schulten, Scalable molecular dynamics with NAMD, J. Comput. Chem. 26 (2005) 1781–1802.
[25] A.D. Mackerell, M. Feig, C.L. Brooks, Extending the treatment of backbone energetics in protein force fields: limitations of gas-phase quantum mechanics in reproducing protein conformational distributions in molecular dynamics simulations, J. Comput. Chem. 25 (2004) 1400–1415.
[26] J. Taylor, N.E. Whiteford, G. Bradley, G.W. Watson, Validation of all-atom phosphatidylcholine lipid force fields in the tensionless NPT ensemble, Biochim. Biophys. Acta 1788 (2009) 638–649.
[27] S. Pöyry, T. Róg, M. Karttunen, I. Vattulainen, Mitochondrial membranes with mono- and divalent salt: changes induced by salt ions on structure and dynamics, J. Phys. Chem. B 113 (2009) 15513–15521.
[28] T. Róg, H. Martinez-Seara, N. Munck, M. Oresic, M. Karttunen, I. Vattulainen, Role of cardiolipins in the inner mitochondrial membrane: insight gained through atom-scale simulations, J. Phys. Chem. B 113 (2009) 3413–3422.
[29] U. Essmann, L. Perera, M.L. Berkowitz, T. Darden, H. Lee, L.G. Pedersen, A smooth particle mesh Ewald method, J. Chem. Phys. 103 (1995) 8577.
[30] K. Kaszuba, T. Róg, K. Bryl, I. Vattulainen, M. Karttunen, Molecular dynamics simulations reveal fundamental role of water as factor determining affinity of binding of beta-blocker nebivolol to beta(2)-adrenergic receptor, J. Phys. Chem. B 114 (2010) 8374–8386.
[31] H. Ding, C.C. Moser, D.E. Robertson, M.K. Tokito, F. Daldal, P.L. Dutton, Ubiquinone pair in the Qo site central to the primary energy conversion reactions of cytochrome bc1 complex, Biochemistry 34 (1995) 15979–15996.
[32] A.R. Crofts, B. Barquera, R.B. Gennis, R. Kuras, M. Guergova-Kuras, E.A. Berry, Mechanism of ubiquinol oxidation by the bc(1) complex: different domains of the quinol binding pocket and their role in the mechanism and binding of inhibitors, Biochemistry 38 (1999) 15807–15826.
[33] S. Bartoschek, M. Johansson, B.H. Geierstanger, J.G. Okun, C.R. Lancaster, E. Humpfer, L. Yu, C.A. Yu, C. Griesinger, U. Brandt, Three molecules of ubiquinone bind specifically to mitochondrial cytochrome bc1 complex, J. Biol. Chem. 276 (2001) 35231–35234.
[34] C. Hunte, J. Koepke, C. Lange, T. Rossmanith, H. Michel, Structure at 2.3 A resolution of the cytochrome bc(1) complex from the yeast Saccharomyces cerevisiae co-crystallized with an antibody Fv fragment, Structure 8 (2000) 669–684.
[35] L.-S. Huang, D. Cobessi, E.Y. Tung, E.A. Berry, Binding of the respiratory chain inhibitor antimycin to the mitochondrial bc1 complex: a new crystal structure reveals an altered intramolecular hydrogen-bonding pattern, J. Mol. Biol. 351 (2005) 573–597.
[36] L. Esser, B. Quinn, Y.-F. Li, M. Zhang, M. Elberry, L. Yu, C.-A. Yu, Di Xia, Crystallographic studies of quinol oxidation site inhibitors: a modified classification of inhibitors for the cytochrome bc(1) complex, J. Mol. Biol. 341 (2004) 281–302.
[37] C. Lange, J.H. Nett, B.L. Trumpower, C. Hunte, Specific roles of protein–phospholipid interactions in the yeast cytochrome bc1 complex structure, EMBO J. 20 (2001) 6591–6600.
[38] L. Esser, M. Elberry, F. Zhou, C.-A. Yu, L. Yu, Di Xia, Inhibitor-complexed structures of the cytochrome bc1 from the photosynthetic bacterium *Rhodobacter sphaeroides*, J. Biol. Chem. 283 (2008) 2846–2857.
[39] S.R.N. Solmaz, C. Hunte, Structure of complex III with bound cytochrome c in reduced state and definition of a minimal core interface for electron transfer, J. Biol. Chem. 283 (2008) 17542–17549.
[40] E.A. Berry, L.-S. Huang, D.-W. Lee, F. Daldal, K. Nagai, N. Minagawa, Ascochlorin is a novel, specific inhibitor of the mitochondrial cytochrome bc1 complex, Biochim. Biophys. Acta 1797 (2010) 360–370.
[41] A.R. Crofts, S. Hong, N. Ugulava, B. Barquera, R. Gennis, M. Guergova-Kuras, E.A. Berry, Pathways for proton release during ubihydroquinone oxidation by the bc(1) complex, Proc. Natl. Acad. Sci. U. S. A. 96 (1999) 10021–10026.
[42] R. Covián, R. Moreno-Sánchez, Role of protonatable groups of bovine heart bc(1) complex in ubiquinol binding and oxidation, Eur. J. Biochem. 268 (2001) 5783–5790.
[43] A. Osyczka, H. Zhang, C. Mathé, P.R. Rich, C.C. Moser, P.L. Dutton, Role of the PEWY glutamate in hydroquinone-quinone oxidation-reduction catalysis in the Qo Site of cytochrome bc1, Biochemistry 45 (2006) 10492–10503.
[44] N. Seddiki, B. Meunier, D. Lemesle-Meunier, G. Brasseur, Is cytochrome b glutamic acid 272 a quinol binding residue in the bc1 complex of Saccharomyces cerevisiae? Biochemistry 47 (2008) 2357–2368.
[45] M. Iwaki, G. Yakovlev, J. Hirst, A. Osyczka, P.L. Dutton, D. Marshall, P.R. Rich, Direct observation of redox-linked histidine protonation changes in the iron-sulfur protein of the cytochrome bc1 complex by ATR-FTIR spectroscopy, Biochemistry 44 (2005) 4230–4237.
[46] U. Brandt, J.G. Okun, Role of deprotonation events in ubihydroquinone:cytochrome c oxidoreductase from bovine heart and yeast mitochondria, Biochemistry 36 (1997) 11234–11240.
[47] S. Izrailev, A.R. Crofts, E.A. Berry, K. Schulten, Steered molecular dynamics simulation of the Rieske subunit motion in the cytochrome bc(1) complex, Biophys. J. 77 (1999) 1753–1768.
[48] J.E. Ladbury, Just add water! The effect of water on the specificity of protein–ligand binding sites and its potential application to drug design, Chem. Biol. 3 (1996) 973–980.
[49] L.R. Olano, S.W. Rick, Hydration free energies and entropies for water in protein interiors, J. Am. Chem. Soc. 126 (2004) 7991–8000.
[50] R. Baron, P. Setny, J.A. McCammon, Water in cavity-ligand recognition, J. Am. Chem. Soc. 132 (2010) 12091–12097.
[51] J.M. Sanders, O.T. Pentikäinen, L. Settimo, U. Pentikäinen, M. Shoji, M. Sasaki, R. Sakai, M.S. Johnson, G.T. Swanson, Determination of binding site residues responsible for the subunit selectivity of novel marine-derived compounds on kainate receptors, Mol. Pharmacol. 69 (2006) 1849–1860.
[52] U. Pentikäinen, L. Settimo, M.S. Johnson, O.T. Pentikäinen, Subtype selectivity and flexibility of ionotropic glutamate receptors upon antagonist ligand binding, Org. Biomol. Chem. 4 (2006) 1058–1070.
[53] P.A. Postila, G.T. Swanson, O.T. Pentikäinen, Exploring kainate receptor pharmacology using molecular dynamics simulations, Neuropharmacology 58 (2010) 515–527.
[54] S.P. Niinivehmas, S.I. Virtanen, J.V. Lehtonen, P.A. Postila, O.T. Pentikäinen, Comparison of virtual high-throughput screening methods for the identification of phosphodiesterase-5 inhibitors, J. Chem. Inf. Model. 51 (2011) 1353–1363.
[55] J.T. Koivunen, L. Nissinen, A. Juhakoski, M. Pihlavisto, A. Marjamäki, J. Huuskonen, O.T. Pentikäinen, Blockage of collagen binding to integrin $\alpha 2\beta 1$: structure–activity relationship of protein–protein interaction inhibitors, Med. Chem. Commun. 2 (2011) 764.
[56] F. Garczarek, K. Gerwert, Functional waters in intraprotein proton transfer monitored by FTIR difference spectroscopy, Nature 439 (2006) 109–112.
[57] D.R.J. Kolling, R.I. Samoilova, J.T. Holland, E.A. Berry, S.A. Dikanov, A.R. Crofts, Exploration of ligands to the Qi site semiquinone in the bc1 complex using high-resolution EPR, J. Biol. Chem. 278 (2003) 39747–39754.
[58] D. Bakowies, W.F. van Gunsteren, Water in protein cavities: a procedure to identify internal water and exchange pathways and application to fatty acid-binding protein, Proteins 47 (2002) 534–545.
[59] A. Borek, M. Sarewicz, A. Osyczka, Movement of the iron-sulfur head domain of cytochrome bc(1) transiently opens the catalytic Q(o) site for reaction with oxygen, Biochemistry 47 (2008) 12365–12370.
[60] F. Muller, A.R. Crofts, D.M. Kramer, Multiple Q-cycle bypass reactions at the Qo site of the cytochrome bc1 complex, Biochemistry 41 (2002) 7866–7874.
[61] A. Osyczka, C.C. Moser, P.L. Dutton, Fixing the Q cycle, Trends Biochem. Sci. 30 (2005) 176–182.
[62] J. Zhu, T. Egawa, S.-R. Yeh, L. Yu, C.-A. Yu, Simultaneous reduction of iron-sulfur protein and cytochrome b(L) during ubiquinol oxidation in cytochrome bc(1) complex, Proc. Natl. Acad. Sci. U. S. A. 104 (2007) 4864–4869.